Hydrogen Evolution

DOI: 10.1002/anie.201406848

A Cost-Effective 3D Hydrogen Evolution Cathode with High Catalytic Activity: FeP Nanowire Array as the Active Phase**

*Ping Jiang, Qian Liu, Yanhui Liang, Jingqi Tian, Abdullah M. Asiri, and Xuping Sun**

Abstract: *Iron is the cheapest and one of the most abundant transition metals. Natural [FeFe]-hydrogenases exhibit remarkably high activity in hydrogen evolution, but they suffer from high oxygen sensitivity and difficulty in scale-up. Herein, an FeP nanowire array was developed on Ti plate (FeP NA/Ti) from its β-FeOOH NA/Ti precursor through a low-temperature phosphidation reaction. When applied as self-supported 3D hydrogen evolution cathode, the FeP NA/Ti electrode shows exceptionally high catalytic activity and good durability, and it only requires overpotentials of 55 and 127 mV to afford current densities of 10 and 100 mA cm^2, respectively. The excellent electrocatalytic performance is promising for applications as non-noble-metal HER catalyst with a high performance–price ratio in electrochemical water splitting for large-scale hydrogen fuel production.*

Hydrogen as a promising clean chemical fuel is an ideal energy carrier for sustainable energy applications.[1] Electrochemical reduction of water for hydrogen production is an important component of several emerging clean-energy technologies, but an efficient electrocatalyst for the hydrogen evolution reaction (HER) is required to afford high current at low overpotential.[2] Although Pt-based catalysts show high catalytic performance, they suffer from high costs and the scarcity of Pt.[3] Water electrolysis based on proton exchange membrane (PEM) technology and many solar water splitting devices operate under strongly acidic conditions,[4] it is thus highly attractive to develop acid-stable HER catalysts made from earth-abundant elements. Catalysts based on Mo, W, and Fe-group elements have received great attention, including MoS_2,[5] $MoSe_2$,[6] MoB,[7] Mo_2C,[7,8] $NiMoN_x$,[9] $Co_{0.6}Mo_{1.4}N_2$,[10] WS_2,[11] $CoSe_2$,[12] CoP,[13] Ni_2P,[14] Cu_3P,[15] and MoP.[16]

Naturally occurring [FeFe]-hydrogenases show remarkably high activity in hydrogen evolution,[17] which has inspired considerable research efforts to develop artificial molecular mimics.[18] However, the hydrogenases suffer from high oxygen sensitivity and difficult scale-up[19] while the mimics suffer from large overpotential and/or low stability.[20] Practical application of the mimics requires their grafting onto current collectors to prepare the electrocatalytic hydrogen evolution cathode,[21] which remains a challenging task because of synthetic issues with such complexes.[22] The design of solid-state inorganic catalysts could offer an alternative strategy.[23] Given that Fe is the cheapest and one of the most abundant transition metals, it is expected that artificial Fe-based solid-state inorganic compounds would represent a cheap HER catalysts. Xu et al. have recently developed FeP nanosheets as a HER catalyst in acidic solution,[24] but this catalyst requires a large overpotential (η) of ca. 240 mV to afford a current density of 10 mA cm^{-2} and its preparation suffers from the involvement of several organic solvents.

In principle, electrochemical tests require the effective immobilization of electrocatalysts of interest on current collectors with the use of a polymer binder as film-forming agent. The polymer binder generally increases the series resistance[25] and may block active sites and inhibit diffusion, leading to reduced catalytic activity.[26] Such issues have been successfully solved by directly growing the active phase on the current collector.[13c,15] Here, we describe further advancement in this direction by developing a FeP nanowire array supported on conductive Ti plate (FeP NA/Ti) as an integrated 3D hydrogen evolution cathode. FeP NA is the active phase and Ti is the current collector. Unexpectedly, the FeP NA/Ti electrode shows exceptionally high catalytic activity and good durability in aicidc media. It exhibits a very small onset overpotential of 16 mV, a low Tafel slope of 38 mV/dec and a large exchange current density of 0.42 mA cm^{-2}. Further, it requires overpotentials of only 55 and 127 mV to afford current densities of 10 and 100 mA cm^{-2}, respectively.

A two-step strategy was used to fabricate FeP NA/Ti. First, FeOOH NA is hydrothermally grown on Ti, followed by chemical conversion of the resulting FeOOH NA/Ti precursor into FeP NA/Ti by a low-temperature phosphidation reaction (see Supporting Information (SI) for details). Figure 1 a and b show the X-ray diffraction (XRD) patterns for FeOOH and the phosphidated product which was scraped off the Ti plate. The Fe precursor shows diffraction peaks characteristic of β-phase FeOOH (JCPDS No. 75-1594)[27]

[*] Dr. P. Jiang,[+] Q. Liu,[+] Y. Liang, Dr. J. Tian, Prof. X. Sun
State Key Laboratory of Electroanalytical Chemistry
Changchun Institute of Applied Chemistry
Changchun 130022, Jilin (China)
E-mail: sunxp@ciac.ac.cn
Q. Liu[+]
College of Chemistry and Chemical Engineering
China West Normal University, Nanchong 637002, Sichuan (China)
Prof. A. M. Asiri
Chemistry Department & Center of Excellence for Advanced Materials Research
King Abdulaziz University, Jeddah 21589 (Saudi Arabia)
[+] These authors contributed equally to this work.

[**] This work was supported by the National Natural Science Foundation of China (No. 21175129) and the National Basic Research Program of China (No. 2011CB935800).
Supporting information for this article is available on the WWW under http://dx.doi.org/10.1002/anie.201406848.

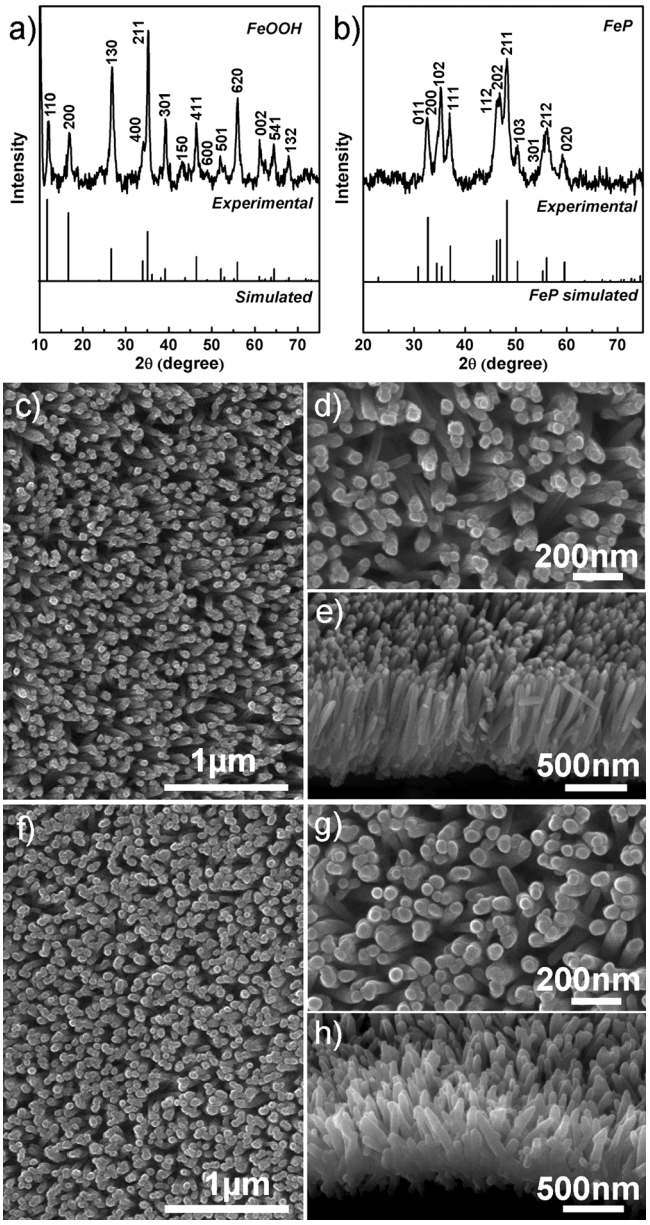

Figure 1. XRD patterns for a) FeOOH and b) FeP scraped off the Ti plate. c) Low- and d) high-magnification SEM images of FeOOH NA/Ti precursor. e) Cross-section SEM image of FeOOH NA/Ti. f) Low- and g) high-magnification SEM images of FeP NA/Ti. h) Cross-section SEM image of FeP NA/Ti.

while the phosphidated product only shows peaks corresponding to FeP (JCPDS No. 78-1443).[28] The XRD intensities do not match exactly with those of the simulated patterns, which could be due to preferred orientation.[29] Figure 1c and d show scanning electron microscopy (SEM) images of FeOOH NA/Ti, indicating full coverage of FeOOH nanowires (FeOOH NWs; 40–80 nm in diameters) on the surface of the Ti plate. Cross-section analysis (Figure 1e) shows that these nanowires are up to 700 nm in length, highly oriented, and uniformly aligned in a dense array with little bending. After phosphidation, the 1D array format remains intact (Figure 1 f–h). Compared to the FeOOH NWs, the FeP NWs have larger diameters (50–95 nm) but decreased lengths (up to 600 nm) with a lower aspect ratio. The energy-dispersive X-ray (EDX) spectrum (Figure S1 in the SI) indicates a 1:1.08 Fe:P ratio in the FeP NWs, consistent within experimental error with the expected 1:1 FeP stoichiometry.

Figure 2a shows transmission electron microscopy (TEM) images of FeP NWs, further confirming the preservation of the 1D morphology in the FeOOH precursor[30] (Figure S2) after phosphidation. A high-resolution TEM (HRTEM)

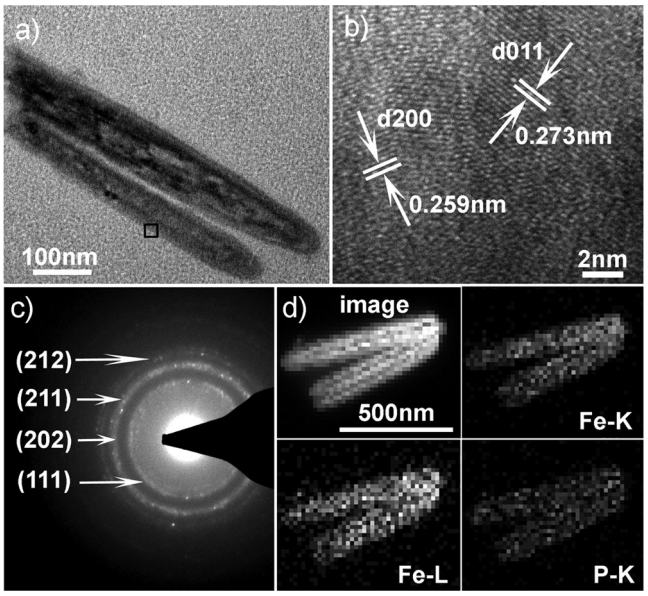

Figure 2. a) TEM image of FeP NWs scraped off the Ti plate. b) HRTEM image taken from the area marked with a black rectangle in (a). c) SAED pattern of FeP NWs. d) STEM image and EDX elemental mapping of Fe and P for FeP NWs.

image of the selected area in Figure 2a shows well-resolved lattice fringes with interplanar distances of 0.273 and 0.259 nm, which can be indexed to the (011) and (200) plane of FeP, respectively (Figure 2b). The corresponding selected-area electron diffraction (SAED) pattern, showing discrete spots indexed to the (111), (202), (211) and (212) planes of orthorhombic FeP (Figure 2c),[28] indicates that FeP is polycrystalline. Figure 2d shows the scanning TEM image (STEM) and EDX elemental mapping images of Fe and P for FeP NWs, clearly confirming that Fe and P elements are uniformly distributed throughout the nanowire. It should be mentioned that the same preparation without using Ti substrate leads to individual β-FeOOH NWs and phosphidation produces FeP NWs (Figure S3).

We examined the electrocatalytic HER activity of FeP NA/Ti (FeP loading: 3.2 mg cm^{-2}) in 0.5 M H_2SO_4 with a scan rate of 2 mV s^{-1}. Commercial Pt/C (20 wt% Pt/XC-72) and blank Ti plate were also examined for comparison. Because as-measured reaction currents do not directly reflect the intrinsic behavior of catalysts due to the effect of ohmic resistance, an *iR* correction was applied to all initial data for further analysis. Figure 3a shows the polarization curves. Pt/C

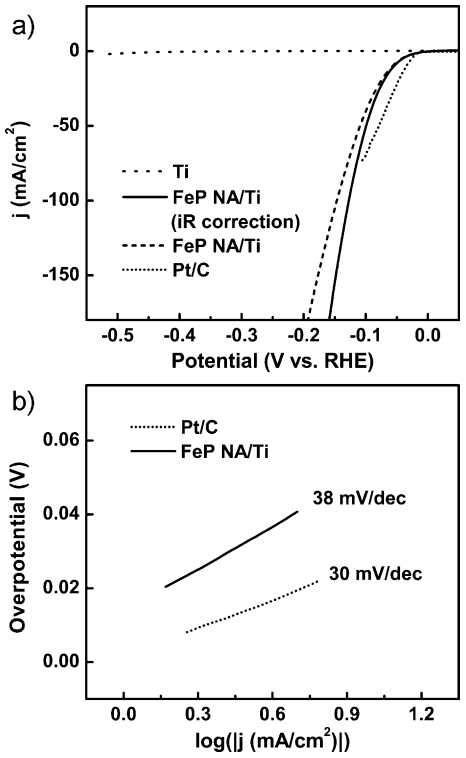

Figure 3. a) Polarization curves for blank Ti plate, Pt/C, and FeP NA/Ti in 0.5 M H_2SO_4 with a scan rate of 2 mV s^{-1}. b) Tafel plots for FeP NA/Ti and Pt/C.

exhibits excellent HER activity with a near-zero overpotential while blank Ti plate shows poor HER activity with an onset overpotential of 430 mV. In sharp contrast, the FeP NA/Ti electrode shows a low onset overpotential of 16 mV, and further negative potential scanning causes a sharp rise of the cathodic current intensity, suggesting superior catalytic activity of FeP NA. Furthermore, this electrode only requires overpotentials of 55, 72, and 127 mV to afford current densities of 10, 20, and 100 mA cm^{-2}, respectively. These overpotentials are the lowest among all reported values for non-noble metal acid-stable HER catalysts including our recently developed CoP/CC,[13c] CoP/Ti,[13d] Ni_2P/Ti,[14c] and Cu_3P NWs/CF[15] hydrogen evolution cathodes (Table S1).

Figure 3b presents Tafel plots, η vs. log(j), for Pt/C and FeP NA/Ti. The Tafel slope 30 mV/dec for Pt/C is consistent with the reported value.[14a] FeP NA/Ti exhibits a Tafel slope of 38 mV/dec in the region $\eta = 20$–40 mV, which is smaller than for all reported non-noble metal HER catalysts except $NiMoN_x$/C in acidic media (Table S1). This Tafel slope indicates that the HER occurs through a Volmer–Heyrovsky mechanism and electrochemical recombination with an additional proton is the rate-limiting step.[12] It should be mentioned that the exchange current density of FeP NA/Ti was determined to be 0.42 mA cm^{-2} by applying an extrapolation method to the Tafel plot (Figure S4), which is the largest value for all non-Pt HER catalysts listed in Table S1.

Note that FeP NWs obtained without the presence of Ti plate can be subsequently immobilized on Ti plate using nafion as binder (FeP NW/Ti, FeP loading: 3.2 mg cm^{-2}). However, in order to attain a current density of 2 mA cm^{-2}, this electrode requires an overpotential of 225 mV (Figure S5a), much larger than the value (26 mV) for FeP NA/Ti. The superior catalytic activity of FeP NA/Ti can be attributed to the following five reasons: 1) The direct growth of FeP on Ti plate ensures intimate contact, good mechanical adhesion and excellent electrical connection between FeP and Ti, leading to an enhanced electron flow from Ti to FeP during cathodic scanning. 2) Transition metal phosphides, as an important class of compounds formed by the alloying of metals and phosphorus, possess high electrical conductivity;[31] this property greatly benefits the electrochemical performance of catalysts and favors fast electron transport along FeP. 3) The 1D array is capable of vectorial electron transport[32] and the open spaces between the nanowires allow for enhanced diffusion of electrolyte and more efficient utilization of active sites.[5b] 4) The high FeP loading leads to improved catalytic efficiency.[13a,33] 5) The binder-free feature of FeP NA/Ti not only leads to improved conductivity,[25] but effectively avoids blocking of active sites and the inhibition of diffusion.[26] Indeed, electrochemical impedance analysis shows that FeP NA/Ti has much lower impedance and thus markedly faster HER kinetics than FeP NW/Ti,[34] as shown in Figure S5b.

We have further investigated the stability of FeP NA/Ti during long-term cycling and continuous HER at a static potential in 0.5 M H_2SO_4. After 1000 continuous cyclic voltammetric (CV) cycles between +0.28 and −0.17 V vs. RHE with a scan rate of 100 mV s^{-1}, the overpotential required to afford a current density of 100 mA cm^{-2} increased by less than 36 mV (Figure 4), much lower than the reported

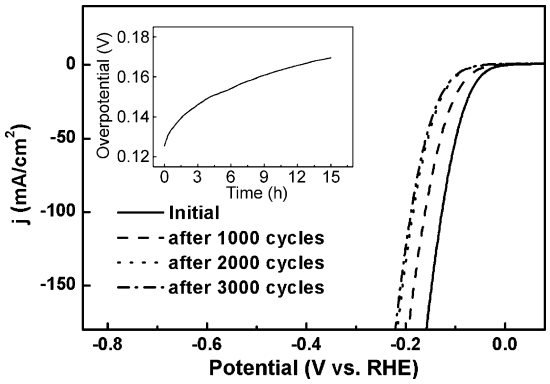

Figure 4. Polarization curves for FeP NA/Ti in 0.5 M H_2SO_4 initially and after 1000, 2000, and 3000 cycles at a scan rate of 100 mV s^{-1} between +0.28 and −0.17 V (inset: plot of overpotential vs. time for FeP NA/Ti electrode at a constant cathodic current density of 90 mA cm^{-2}).

50 mV for Ni_2P hollow nanoparticles deposited on Ti plate after 500 CV sweeps.[14a] After 2000 and 3000 CV sweeps, the overpotential required increased by 63 mV. SEM observations demonstrate that the FeP NA/Ti preserves its 3D configuration and morphological integrity after CV cycling (Figure S6a–c). A close TEM examination revealed that the FeP surface became much rougher (Figure S6d) but retained FeP in composition and structure (Figure S6e and f), suggest-

ing the occurrence of some corrosion.[14] Figure 4 inset shows galvanostatic measurements at a current density of 90 mA cm^{-2} in 0.5 M H_2SO_4, suggesting that the overpotential increases by less than 45 mV over 15 h of continuous operation. These results demonstrate good acidic stability of the FeP NA/Ti electrode. In addition, the Faradaic efficiency (FE) for hydrogen evolution of this electrode was determined to be nearly 100% in acidic electrolytes by using a method reported elsewhere[13b–e,14c,15,16a] (Figure S7).

Figure S8 shows the X-ray photoelectron spectroscopy (XPS) 2p spectra in the Fe($2p_{3/2}$) and P(2p) regions for FeP NA/Ti. The peaks for the binding energy (BE) of Fe $2p_{3/2}$ appear at 707.1 and 710.5 eV. The high-resolution P(2p) region shows two peaks at 130.2 and 129.3 eV reflecting the BE of P $2p_{1/2}$ and P $2p_{3/2}$, respectively, along with one peak at 133.4 eV. The peaks at 707.1 and 129.3 eV are close to the BE for Fe and P in FeP.[35] The peaks at 710.5 and 133.4 eV can be assigned to oxidized Fe and P species arising from superficial oxidation of FeP exposed to air.[36] Note that the FeOOH precursor shows a Fe $2p_{3/2}$ peak at 711.4 eV (Figure S9), which is consistent with previous report[37] and deviated from the BE (710.5 eV) of Fe $2p_{3/2}$ for oxidized Fe species in FeP. The XPS depth profiling analysis (Figure S10) indicates that the change of content of both Fe and P elements from the FeP NWs is very small during Ar^+ etching, suggesting homogeneous distribution of both elements inside the nanowire[38] and complete chemical conversion of FeOOH into FeP. The Fe 2p BE of 707.1 eV is positively shifted from that of metallic Fe (706.8 eV)[39] while the P 2p BE of 129.3 eV shows negative shift from that of elemental P (130.2 eV),[40] suggesting Fe and P in FeP NWs carry partial positive charge (δ^+) and negative charge (δ^-), respectively. The results imply the occurrence of electron transfer from Fe to P in FeP,[35,36,41] which is consistent with our previous observations for CoP, Cu_3P and MoP.[13b–e,15,16a] The active sites in hydrogenase feature pendant bases proximate to the metal centers[42] and metal complex HER catalysts also incorporate proton relays from pendant acid/base groups positioned close to the metal center where hydrogen evolution occurs.[43] In our present study, FeP also features pendant base P (δ^-) positioned close to metal center Fe (δ^+), and therefore, we may suggest that both Fe center and the pendant base P are the active sites for the hydrogen evolution. The Fe and P act as the hydride acceptor and proton acceptor center, respectively, facilitating the HER.[14a,44] Further, P could facilitate the formation of Fe-hydride for subsequent hydrogen evolution via electrochemical desorption.[45]

In conclusion, an FeP nanowire array was prepared on Ti plate through low-temperature phosphidation of a β-FeOOH NA/Ti precursor. The resulting FeP NA/Ti 3D hydrogen evolution cathode exhibits exceptionally high catalytic activity and good stability in acidic electrolytes. The wide availability of Fe, its easy low-cost and scalable fabrication process, and the high catalytic activity promise its use as an integrated 3D cathode with highest performance–price ratio in electrochemical water splitting for large-scale hydrogen fuel production.[46]

Received: July 3, 2014
Revised: August 21, 2014
Published online: September 24, 2014

Keywords: electrocatalysis · FeP nanowires · hydrogen evolution · water splitting

[1] a) T. J. Meyer, *Acc. Chem. Res.* **1989**, *22*, 163–170; b) J. A. Turner, *Science* **2004**, *305*, 972–974; c) H. B. Gray, *Nat. Chem.* **2009**, *1*, 7–7.
[2] M. G. Walter, E. L. Warren, J. R. McKone, S. W. Boettcher, Q. Mi, E. A. Santori, N. S. Lewis, *Chem. Rev.* **2010**, *110*, 6446–6473.
[3] a) J. Greeley, J. K. Norskov, L. A. Kibler, A. M. El-Aziz, D. M. Kolb, *ChemPhysChem* **2006**, *7*, 1032–1035; b) W. C. Sheng, H. A. Gasteiger, Y. Shao-Horn, *J. Electrochem. Soc.* **2010**, *157*, B1529–B1536.
[4] a) A. Le Goff, V. Artero, B. Jousselme, P. D. Tran, N. Guillet, R. Métayé, A. Fihri, S. Palacin, M. Fontecave, *Science* **2009**, *326*, 1384–1387; b) M. Hambourger, M. Gervaldo, D. Svedruzic, P. W. King, D. Gust, M. Ghirardi, A. L. Moore, T. A. Moore, *J. Am. Chem. Soc.* **2008**, *130*, 2015–2022; c) D. Kong, H. Wang, Z. Lu, Y. Cui, *J. Am. Chem. Soc.* **2014**, *136*, 4897–4900.
[5] a) T. F. Jaramillo, K. P. Jørgensen, J. Bonde, J. H. Nielsen, S. Horch, I. Chorkendorff, *Science* **2007**, *317*, 100–102; b) J. Kibsgaard, Z. Chen, B. N. Reinecke, T. F. Jaramillo, *Nat. Mater.* **2012**, *11*, 963–969; c) M. A. Lukowski, A. S. Daniel, F. Meng, A. Forticaux, L. Li, S. Jin, *J. Am. Chem. Soc.* **2013**, *135*, 10274–10277; d) J. Xie, H. Zhang, S. Li, R. Wang, X. Sun, M. Zhou, J. Zhou, X. Lou, Y. Xie, *Adv. Mater.* **2013**, *25*, 5807–5813.
[6] D. Kong, H. Wang, J. J. Cha, M. Pasta, K. J. Koski, J. Yao, Y. Cui, *Nano Lett.* **2013**, *13*, 1341–1347.
[7] H. Vrubel, X. Hu, *Angew. Chem. Int. Ed.* **2012**, *51*, 12703–12706; *Angew. Chem.* **2012**, *124*, 12875–12878.
[8] a) W. Chen, C. Wang, K. Sasaki, N. Marinkovic, W. Xu, J. T. Muckerman, Y. Zhu, R. R. Adzic, *Energy Environ. Sci.* **2013**, *6*, 943–951; b) C. Wan, Y. N. Regmi, B. M. Leonard, *Angew. Chem. Int. Ed.* **2014**, *53*, 6407–6410; *Angew. Chem.* **2014**, *126*, 6525–6528.
[9] W. Chen, K. Sasaki, C. Ma, A. I. Frenkel, N. Marinkovic, J. T. Muckerman, Y. Zhu, R. R. Adzic, *Angew. Chem. Int. Ed.* **2012**, *51*, 6131–6135; *Angew. Chem.* **2012**, *124*, 6235–6239.
[10] B. Cao, G. M. Veith, J. C. Neuefeind, R. R. Adzic, P. G. Khalifah, *J. Am. Chem. Soc.* **2013**, *135*, 19186–19192.
[11] a) D. Voiry, H. Yamaguchi, J. Li, R. Silva, D. C. B. Alves, T. Fujita, M. Chen, T. Asefa, V. B. Shenoy, G. Eda, M. Chhowalla, *Nat. Mater.* **2013**, *12*, 850–855; b) J. Yang, D. Voiry, S. J. Ahn, D. Kang, A. Y. Kim, M. Chhowalla, H. S. Shin, *Angew. Chem. Int. Ed.* **2013**, *52*, 13751–13754; *Angew. Chem.* **2013**, *125*, 13996–13999; c) L. Cheng, W. Huang, Q. Gong, C. Liu, Z. Liu, Y. Li, H. Dai, *Angew. Chem. Int. Ed.* **2014**, *53*, 7860–7863; *Angew. Chem.* **2014**, *126*, 7994–7997.
[12] a) Y. Xu, M. Gao, Y. Zheng, J. Jiang, S. Yu, *Angew. Chem. Int. Ed.* **2013**, *52*, 8546–8550; *Angew. Chem.* **2013**, *125*, 8708–8712; b) D. Kong, H. Wang, Z. Lu, Y. Cui, *J. Am. Chem. Soc.* **2014**, *136*, 4897–4900.
[13] a) E. J. Popczun, C. G. Read, C. W. Roske, S. Lewis, R. E. Schaak, *Angew. Chem. Int. Ed.* **2014**, *53*, 5427–5430; *Angew. Chem.* **2014**, *126*, 5531–5534; b) Q. Liu, J. Tian, W. Cui, P. Jiang, N. Cheng, A. M. Asiri, X. Sun, *Angew. Chem. Int. Ed.* **2014**, *53*, 6710–6714; *Angew. Chem.* **2014**, *126*, 6828–6832; c) J. Tian, Q. Liu, A. M. Asiri, X. Sun, *J. Am. Chem. Soc.* **2014**, *136*, 7587–7590; d) Z. Pu, Q. Liu, P. Jiang, A. M. Asiri, A. Y. Obaid, X. Sun, *Chem. Mater.* **2014**, *26*, 4326–4329; e) P. Jiang, Q. Liu, C. Ge, W. Cui, Z. Pu, A. M. Asiri, X. Sun, *J. Mater. Chem. A* **2014**, *2*, 14634–14640.

[14] a) E. J. Popczun, J. R. McKone, C. G. Read, A. J. Biacchi, A. M. Wiltrout, N. S. Lewis, R. E. Schaak, *J. Am. Chem. Soc.* **2013**, *135*, 9267 – 9270; b) L. Feng, H. Vrubel, M. Bensimon, X. Hu, *Phys. Chem. Chem. Phys.* **2014**, *16*, 5917 – 5921; c) Z. Pu, Q. Liu, C. Tang, A. M. Asiri, X. Sun, *Nanoscale* **2014**, *6*, 11031 – 11034.

[15] J. Tian, Q. Liu, N. Cheng, A. M. Asiri, X. Sun, *Angew. Chem. Int. Ed.* **2014**, *53*, 9577 – 9581; *Angew. Chem.* **2014**, *126*, 9731 – 9735.

[16] a) Z. Xing, Q. Liu, A. M. Asiri, X. Sun, *Adv. Mater.* **2014**, *26*, 5702 – 5707; b) P. Xiao, M. A. Sk, L. Thia, X. Ge, R. J. Lim, J. Wang, K. H. Lim, X. Wang, *Energy Environ. Sci.* **2014**, *7*, 2624 – 2629; c) J. M. McEnaney, J. C. Crompton, J. F. Callejas, E. J. Popczun, A. J. Biacchi, N. S. Lewis, R. E. Schaak, *Chem. Mater.* **2014**, *26*, 4826 – 4831.

[17] a) L. Ghirardi, A. Dubini, J. Yu, P. C. Maness, *Chem. Soc. Rev.* **2009**, *38*, 52 – 61; b) N. Wang, M. Wang, L. Chen, L. Sun, *Dalton Trans.* **2013**, *42*, 12059 – 12071.

[18] a) S. Ott, M. Kritikos, B. Åkermark, L. Sun, *Angew. Chem. Int. Ed.* **2003**, *42*, 3285 – 3288; *Angew. Chem.* **2003**, *115*, 3407 – 3410; b) L. Song, M. Tang, F. Su, Q. Hu, *Angew. Chem. Int. Ed.* **2006**, *45*, 8126 – 8130; *Angew. Chem.* **2006**, *118*, 8306 – 8310; c) C. Tard, C. J. Pickett, *Chem. Rev.* **2009**, *109*, 2245 – 2274.

[19] J. A. Cracknell, K. A. Vincent, F. A. Armstrong, *Chem. Rev.* **2008**, *108*, 2439 – 2461.

[20] V. Artero, M. Fontecave, *Chem. Soc. Rev.* **2013**, *42*, 2338 – 2356.

[21] P. D. Tran, A. Le Goff, J. Heidkamp, B. Jousselme, N. Guillet, S. Palacin, H. Dau, M. Fontecave, V. Artero, *Angew. Chem. Int. Ed.* **2011**, *50*, 1371 – 1374; *Angew. Chem.* **2011**, *123*, 1407 – 1410.

[22] V. Artero, M. Chavarot-Kerlidou, M. Fontecave, *Angew. Chem. Int. Ed.* **2011**, *50*, 7238 – 7266; *Angew. Chem.* **2011**, *123*, 7376 – 7405.

[23] Y. Sun, C. Liu, D. C. Grauer, J. Yano, J. R. Long, P. Yang, C. J. Chang, *J. Am. Chem. Soc.* **2013**, *135*, 17699 – 17702.

[24] Y. Xu, R. Wu, J. Zhang, Y. Shi, B. Zhang, *Chem. Commun.* **2013**, *49*, 6656 – 6658.

[25] Y. Luo, J. Jiang, W. Zhou, H. Yang, J. Luo, X. Qi, H. Zhang, D. Y. W. Yu, C. M. Li, T. Yu, *J. Mater. Chem.* **2012**, *22*, 8634 – 8640.

[26] J. D. Roy-Mayhew, G. Boschloo, A. Hagfeldt, I. A. Aksay, *ACS Appl. Mater. Interfaces* **2012**, *4*, 2794 – 2800.

[27] D. Qin, C. Tao, S. In, Z. Yang, T. Mallouk, N. Bao, C. A. Grimes, *Energy Fuels* **2011**, *25*, 5257 – 5263.

[28] C. Qian, F. Kim, L. Ma, F. Tsui, P. Yang, J. Liu, *J. Am. Chem. Soc.* **2004**, *126*, 1195 – 1198.

[29] L. B. McCusker, *Microporous Mesoporous Mater.* **1998**, *22*, 527 – 529.

[30] Y. Xiong, Y. Xie, S. Chen, Z. Li, *Chem. Eur. J.* **2003**, *9*, 4991 – 4996.

[31] a) S. T. Oyama, T. Gott, H. Zhao, Y. K. Lee, *Catal. Today* **2009**, *143*, 94 – 107; b) S. Carenco, D. Portehault, C. Boissière, N. Mèzailles, C. Sanchez, *Chem. Rev.* **2013**, *113*, 7981 – 8065.

[32] J. Liao, D. Higgins, G. Lui, V. Chabot, X. Xiao, Z. Chen, *Nano Lett.* **2013**, *13*, 5467 – 5473.

[33] W. Zhou, X. Wu, X. Cao, X. Huang, C. Tan, J. Tian, H. Liu, J. Wang, H. Zhang, *Energy Environ. Sci.* **2013**, *6*, 2921 – 2924.

[34] C. Guo, L. Zhang, J. Miao, J. Zhang, C. M. Li, *Adv. Energy Mater.* **2013**, *3*, 167 – 171.

[35] A. P. Grosvenor, S. D. Wik, R. G. Cavell, A. Mar, *Inorg. Chem.* **2005**, *44*, 8988 – 8998.

[36] L. Li, C. Chen, L. Chen, Z. Zhu, J. Hu, *Environ. Sci. Technol.* **2014**, *48*, 3372 – 3377.

[37] I. D. Welsh, P. M. A. Sherwood, *Phys. Rev. B* **1989**, *40*, 6386 – 6392.

[38] C. Lü, Z. Cui, Y. Wang, Z. Li, C. Guan, B. Yang, J. Shen, *J. Mater. Chem.* **2003**, *13*, 2189 – 2195.

[39] B. Rajesh, N. Sasirekha, S. Lee, H. Kuo, Y. Chen, *J. Mol. Catal. A* **2008**, *289*, 69 – 75.

[40] *Practical Surface Analysis by Auger and X-ray Photoelectron Spectroscopy* (Eds.: D. Briggs, M. P. Seah), Wiley, New York, **1983**.

[41] *Encyclopedia of Inorganic Chemistry*, 2ednd ed(Ed.: R. B. King), Wiley, Hoboken, **2005**.

[42] Y. Nicolet, A. L. Lacey, X. Vérnede, V. M. Fernandez, E. C. Hatchikian, J. C. Fontecilla-Camps, *J. Am. Chem. Soc.* **2001**, *123*, 1596 – 1601.

[43] a) A. D. Wilson, R. H. Newell, M. J. McNevin, J. T. Muckerman, M. R. Dubois, D. L. Dubois, *J. Am. Chem. Soc.* **2006**, *128*, 358 – 366; b) A. D. Wilson, R. K. Shoemaker, A. Miedaner, J. T. Muckerman, D. L. Dubois, M. R. Dubois, *Proc. Natl. Acad. Sci. USA* **2007**, *104*, 6951 – 6956; c) B. E. Barton, T. B. Rauchfuss, *J. Am. Chem. Soc.* **2010**, *132*, 14877 – 14885.

[44] P. Liu, J. A. Rodriguez, *J. Am. Chem. Soc.* **2005**, *127*, 14871 – 14878.

[45] W. Zhang, J. Hong, J. Zheng, Z. Huang, J. Zhou, R. Xu, *J. Am. Chem. Soc.* **2011**, *133*, 20680 – 20683.

[46] During revision of this manuscript, a paper reporting on FeP arrays as a hydrogen evolution catalyst has been published online (August 20, 2014): R. Liu, S. Gu, H. Du, C. M. Li, *J. Mater. Chem. A* **2014**, DOI: 10.1039/c4ta03638g.

